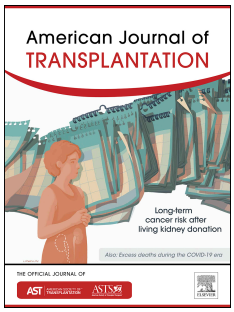

Exploring kidney allograft rejection: A proof-of-concept study using spatial transcriptomics

Cristina Martin-Martin, Beatriz Suarez-Alvarez, Monika González, Irina B. Torres, Oriol Bestard, José E. Martín, Gwendolyn Barceló-Coblijn, Francesc Moreso, Ana M. Aransay, Carlos Lopez-Larrea, Ramon M. Rodriguez

PII: S1600-6135(24)00287-9

DOI: https://doi.org/10.1016/j.ajt.2024.04.015

Reference: AJT 512

To appear in: *American Journal of Transplantation*

Received Date: 6 November 2023

Revised Date: 25 April 2024

Accepted Date: 25 April 2024

Please cite this article as: Martin-Martin C, Suarez-Alvarez B, González M, Torres IB, Bestard O, Martín JE, Barceló-Coblijn G, Moreso F, Aransay AM, Lopez-Larrea C, Rodriguez RM, Exploring kidney allograft rejection: A proof-of-concept study using spatial transcriptomics, *American Journal of Transplantation*, https://doi.org/10.1016/j.ajt.2024.04.015.

Exploring kidney allograft rejection: A proof-of-concept study using spatial transcriptomics

Cristina Martin-Martin[1,2], Beatriz Suarez-Alvarez[1,2], Monika González[3], Irina B. Torres[4], Oriol Bestard[4], José E. Martín[3], Gwendolyn Barceló-Coblijn[5,6], Francesc Moreso[4], Ana M. Aransay[3,7], Carlos Lopez-Larrea[1, 2, 8, *], Ramon M. Rodriguez[5,6].

[1] Translational Immunology, Health Research Institute of the Principality of Asturias (ISPA), Avenida de Roma S/N, 33011, Oviedo, Asturias, Spain.

[2] RICORS2040, Madrid, Spain.

[3] CIC bioGUNE, Basque Research and Technology Alliance (BRTA), Bizkaia Technology Park, 801 bld., 48160, Derio, Bizkaia, Spain.

[4] Department of Nephrology, Hospital Universitari Vall d'Hebron, Nephrology and Renal Transplant Laboratory. Vall Hebron Research Institute (VHIR). Department of Medicine. Autonomous University of Barcelona. Barcelona, Spain.

[5] Lipids in Human Pathology, Institut d'Investigació Sanitària Illes Balears (IdISBa), Ctra. Valldemossa 79, E-07120 Palma, Balearic Islands, Spain.

[6] Research Unit, University Hospital Son Espases, Ctra. Valldemossa79, E-07120 Palma, Balearic Islands, Spain.2. Research Unit, University Hospital Son Espases, Ctra. Valldemossa79, E-07120 Palma, Balearic Islands, Spain.

[7] Centro de Investigación Biomédica en Red de Enfermedades Hepáticas y Digestivas (CIBERehd), Madrid, Spain.

[8] Department of Immunology, Hospital Universitario Central de Asturias, 33011, Oviedo, Spain.

* corresponding author: inmuno@hca.es

3000 words

CADI: Chronic Allograft Damage Index; IFTA: interstitial fibrosis and tubular atrophy; IGTs: immunoglobulin transcripts; GSEA: Gene Set Enrichment Analysis; RT: Renal transplantation; ST: Spatial transcriptomics; UMI: Unique Molecular Identifier

ABSTRACT

In this proof-of-concept study, spatial transcriptomics combined with public single-cell RNA-sequencing data were used to explore the potential of this technology to study kidney allograft rejection. We aimed to map gene expression patterns within diverse pathological states by examining biopsies classified across non-rejection, T cell-mediated acute rejection, and interstitial fibrosis and tubular atrophy (IFTA). Our results revealed distinct immune cell signatures, including those of T and B lymphocytes, monocytes, mast cells, and plasma cells, and their spatial organization within the renal interstitium. We also mapped chemokine receptors and ligands to study immune-cell migration and recruitment. Finally, our analysis demonstrated differential spatial enrichment of transcription signatures associated with kidney allograft rejection across various biopsy regions. Interstitium regions displayed higher enrichment scores for rejection-associated gene expression patterns than did tubular areas, which had negative scores. This implies that these signatures are primarily driven by processes unfolding in the renal interstitium. Overall, this study highlights the value of spatial transcriptomics for revealing cellular heterogeneity and immune signatures in renal transplant biopsies, and demonstrates its potential for studying the molecular and cellular mechanisms associated with rejection. However, certain limitations must be borne in mind regarding the development and future applications of this technology.

INTRODUCTION

Renal transplantation (RT) is the best treatment for end-stage renal disease.[1] The prevention of acute rejection episodes and management of patients has progressed remarkably in recent decades, but the issue of graft loss persists.[2] Strategies are needed to improve the results of RT, and to this end, it is essential to identify the causes of graft loss and recipient death.

The kidney is composed of heterogeneous groups of epithelial, endothelial, immune, and stromal cells, all in close anatomical proximity. Loss of spatial information has been a key limitation of the transcriptomic studies published so far. Spatial transcriptomics (ST) can provide the critical link in this context between classic gene expression and single-cell RNA sequencing; it allows the interrogation of *in situ* expression signatures overlaid upon a histological image. ST methods retain the spatial location of the captured transcripts by incorporating spatial barcode information with no need for tissue homogenization, cell dissociation, or lysis during sample preparation. ST may help us discover or clarify key mechanistic processes within RT that can be therapeutically targeted.[3]

In the present study, we employed a different ST platform combined with publicly available scRNA-seq data in complete samples to gain deeper insights into the molecular landscape using kidney allograft biopsies classified as non-rejection, T cell-mediated acute rejection, and interstitial fibrosis and tubular atrophy (IFTA).

METHODS

Patients and samples

Post-implantation biopsies from deceased kidney donors were OCT-embedded and stored at −80°C (Nephrology Department, Vall d'Hebron Hospital, Barcelona). The present study has been approved by the Vall d'Hebron University Hospital's Clinical Research Ethics Committee (PR(AG)369/2014). All participants signed a written informed consent. The study was conducted following the Declaration of Helsinki and adhered to the Principles of the Declaration of Istanbul on Organ Trafficking and Transplant Tourism. Biopsy specimens were collected in accordance with previously published protocols.[4] The classification of these biopsies according to the BANFF criteria is provided in detail in **Supplemental Table S1**.[5]

Tissue preparation

OCT blocks were cut with a pre-cooled cryostat at 10-µm thickness, and sections were transferred to fit the 6.5-mm^2 oligo-barcoded capture areas on the Visium 10x Genomics slide. Visium Spatial Tissue Optimization was performed according to the 10x Genomics ST Tissue Optimization Manual (CG000238 Rev B), and the fluorescent footprint was imaged using an Olympus BX microscope. An optimal permeabilization time of 22 min was selected. The experimental slide with kidney allograft tissues were dried at 37°C for 1 min, fixed in pre-chilled 100% methanol at −20°C for 30 min, and stained in Mayer's hematoxylin (Sigma–Aldrich Pty. Ltd., Australia) for 7 min and eosin (Dako, Agilent Technologies, Inc., USA) for 5 min. Stained samples were collected as mosaics of 40× fields on an Easy brightfield slide scanner (Motic).

Sequencing library preparation and analysis.

Sequencing libraries were prepared following the Visium Spatial Gene Expression Reagent Kits (CG000239 Rev E) user guide and using a Visium Spatial Gene Expression Slide & Reagent Kit and a Dual Index Kit TT Set A. Following permeabilization and amplification, cDNA was purified, and

cDNA sequencing libraries were prepared. Finally, libraries were quantified using Qubit dsDNA HS DNA Kit (Thermo Fisher Scientific, Cat. # Q32854), visualized on an Agilent 2100 Bioanalyzer using an Agilent High Sensitivity DNA kit (Agilent Technologies, Cat. # 5067-4626) and sequenced using a Novaseq 6000 system (Illumina Inc.) that targeted a minimum of 50,000 read pairs per tissue covered spot on the Capture Area.

Samples were aligned to the hg38 human reference genome. Counts were separated by cell, and the data were filtered and processed using Space Ranger version 1.3.1 according to the manufacturer's specifications.[6] Tissue samples were inspected manually before data processing using the Loupe Browser version 6.0.0 (https://www.10xgenomics.com/products/loupe-browser). Upon analysis, the median number of genes per spot was determined for each biopsy type: 984 in rejection A, 4624 in rejection B, 503 in IFTA, and 674 in non-rejection.

Integration of single-cell RNA-sequencing cell signatures into ST analysis of renal transplant biopsies

Single-cell RNA sequencing data were obtained and unsupervised clustering analysis was carried out on human kidney allograft biopsy tissue using the methods described in an earlier publication.[7] Briefly, the R package Seurat and the FindCluster function were used to cluster cells and extract each cell type's expression markers. Gene expression signatures of each cell type were generated from these data. For our analysis, mitochondrial genes were removed from all gene expression lists due to the over-enrichment observed in the rejection sample, creating an artefactual enrichment in regions of tissue damage within the biopsy. Gene Set Enrichment Analysis (GSEA) (http://software.broadinstitute.org/gsea/index.jsp) and GSEA software 4.3.2 was used to estimate the enrichment of each cell. We used the median normalized average UMI count in each cluster generated by Space Ranger as an expression dataset and each cell expression signature as a gene set input. A total of 10,000 gene set permutations was used. Enrichment of the expression signatures is represented as a normalized enrichment score (NES).[8] Spatial cell co-localization was analyzed using pairwise Pearson correlations. Logarithmically normalized average expression was calculated for each expression cell signature in each spot. Subsequently, we used these coefficients to compile a correlation matrix derived from the pairwise comparisons of the signatures across all samples.

Analysis of transcriptional gene expression signatures associated with kidney allograft rejection

We selected previously reported gene expression signatures relevant to kidney allograft rejection. A TCMR signature was derived from Halloran et al.'s microarray analysis of 703 biopsies (TVEEA algorithm).[9] We also incorporated a signature from Chamoun et al., generated from the microarray analysis of 96 biopsies.[10] Furthermore, we used O'Connell et al.'s expression signature of 25 genes correlated with a high Chronic Allograft Damage Index (CADI ≥ 2) from 204 prospectively collected renal allograft recipients,[11] and a transcriptional signature from Shaw et al. that was positively associated with rejection.[12] Finally, we used a 114-gene signature associated with TCMR,[13] a pan-tissue rejection signature of 102 genes,[14] and an IFTA-associated signature with the top 100 overexpressed genes.[15] GSEA analysis was conducted as previously indicated.

RESULTS

Revealing spatial organization of gene expression in human kidney allograft biopsies through ST mapping

We examined four biopsies with different histological phenotypes (**Table S1**) and diagnostic including acute cellular rejection, IFTA, and unaltered (non-rejection). First, we performed spatially resolved transcriptomic analysis on H&E-stained sections, obtaining a transcriptomic map composed of a set of "spots" with their own unique expression signatures (Figure 1A). Each spot was 55 µm in diameter, and they were localized on the kidney histological image with barcodes. We used segmentation analysis to obtain five unsupervised clusters in the unaltered biopsy, six in the acute rejection biopsy A, and four in the acute rejection biopsy B. The resulting clusters were overlaid seamlessly upon observable histological features (**Supplemental Figure S1**). They were assigned based on known marker genes associated with kidney structures (**Figure 1B**). It is important to highlight that the size of the spots employed in ST analysis can affect the number of cell numbers scored, which varied from one to ten per spot. As a result, some clusters showed a mixed contribution of tubular markers, such as *CALB*, *RHCG*, and *DEFB1*. Furthermore, analysis of the rejection biopsy A revealed a cluster with elevated expression levels of tubular markers, including SLC5A12, and numerous mitochondrial genes located in regions where tubular damage was present. As heightened mitochondrial transcript expression has been widely associated with cellular damage and death,[16] this particular cluster was labelled "tubulitis and cell death". One of the clusters in rejection biopsy B predominantly exhibited elevated expression levels of immunoglobulin genes and was designated as "Plasma cell-enriched". The unaltered biopsy showed a large cluster corresponding to the wall of an artery and other vascular structures.

The validity of the results was corroborated by leveraging cluster markers previously reported through ST analysis of a human kidney biopsy.[17] Our data showed a notable correlation with published signatures, particularly in the context of rejection (**Supplemental Figure S2**).

Investigating the spatial organization and distribution of immune cell subpopulations

We further investigated specific immune cell subpopulations and their spatial distribution within the biopsies using single-cell RNA-sequencing data obtained from a human kidney allograft biopsy.[7] Marker genes for each cell population were obtained to generate cell-specific gene expression signatures. A comprehensive list of genes in each signature is provided in **Supplemental Table S2**. By carrying out GSEA, we were able to derive an enrichment score for each expression signature in our unsupervised cluster analysis. Unsurprisingly, immune cell density in the renal interstitium was significantly higher than in tubular regions, as confirmed by enrichment scores. On the other hand, enrichment scores were generally higher in rejection samples, particularly for plasma cell populations (**Table 1**) (**Figure 2A**). However, this heightened expression was predominantly manifested in the interstitial regions.

In general, the expression of specific immune cell markers was more intense and widely dispersed across the rejection tissue sections than in the non-rejection sample. This was particularly evident in the rejection biopsy B, in which a marked rise in interstitial inflammation was noted **(Figure 2B** and **Supplemental Table S1**). Of the cell markers observed, the expression of T cell markers, such as CD3E, was prominently elevated. Likewise, markers for immunoglobulins (including JCHAIN and IGKC), macrophages (CD163), and non-classic

monocytes (FCGR3A) exhibited higher levels of expression in these rejection samples. Additionally, evidence of mastocyte presence, indicated by TPSAB1 markers, was found in rejection biopsy B.

Next, we aimed to determine whether immune cells exhibit discernible patterns of co-occurrence or dispersion within renal transplant biopsies that would shed light on their functional relationships. To this end, we analyzed the degree of correlation between gene signatures in each spot throughout the tissue sections. Given that each spot captures a small area that contains from 1 to 10 cells approximately, we anticipated that strong correlations in gene expression profiles would signify spatial co-occurrence of these cells. We also examined different tubule cell types, fibroblast, myofibroblast, and endothelial cells in our analysis. All expression signatures were sourced from previously conducted single-cell RNA-sequencing analyses of human kidney allografts.[7] In general, we observed strong positive correlations between some immune cell populations, especially in rejection, and a negative correlation between immune and tubular cells (**Figure 3A**). Nonetheless, transcriptional signatures associated with plasma cells showed weaker correlations with other immune cells, indicating compartmentalization or localization of plasma cells within specific niches within the renal interstitium. In fact, when we visualized the spatial distribution of the transcriptional signatures of B, T, and plasma cells, this phenomenon could be easily observed in the rejection samples, suggesting a particular compartmentalization pattern (**Figure 3B**). Furthermore, our analysis revealed that immunoglobulin genes displayed remarkably high Moran's I spatial autocorrelation values compared with other gene signatures (**Supplemental Figure S3**). Moran's I measures the correlation of gene expression among neighboring spots,[18] so this finding suggests that immunoglobulin-expressing cells tend to cluster together and exert their functional effects in localized areas.

Finally, we compared whether using different single-cell expression data sets could give rise to different spatial distributions of cell populations when integrated with ST data. For this purpose, we contrasted our initial data set with data acquired from the Kidney Precision Medicine Project (KPMP) consortium (**Supplemental Figure S4**).[19] In general, we found a close correlation between signatures, although small differences were observed between samples, indicating that data-source variability can influence spatial distribution.

ST patterns associated with interstitial fibrosis and tubular atrophy

We shifted our focus onto a renal transplant biopsy sample characterized by inflammation within regions of interstitial fibrosis and tubular atrophy (i-IFTA). Unsupervised segmentation analysis yielded a relatively simple clustering structure with only two clusters (**Figure 4A**). Regardless, the expression patterns indicated that one cluster exhibited distinctive enrichment in genes associated with the extracellular matrix and fibroblasts (**Figure 4B**). Next, we examined the distribution of immune cell transcriptional signatures within the IFTA sample. We began by identifying regions of interstitial fibrosis and confirmed their high degree of enrichment of the fibroblast transcriptional signature (**Figure 4C**) which significantly overlapped with immune cell populations, particularly B and T cells. We once more observed a robust spatial correlation among immune cells, mirroring our previous findings in other samples (**Figure 4D**).

In addition, we analyzed published signatures associated with kidney senescence. This approach was motivated by the mounting evidence linking fibrosis to progressive kidney damage and dysfunction. To this end, we evaluated the enrichment of a gene expression signature

associated with kidney senescence derived from the Mouse Ageing Cell Atlas[20] and a human kidney-aging signature (**Figure 4E**).[21] Our results demonstrated that the upregulated genes of the senescence-associated signature attained a notably positive enrichment score within the fibrotic cluster. Conversely, the downregulated genes displayed much lower enrichment scores, reflecting their reduced expression in relation to areas of interstitial fibrosis.

Lastly, because hypoxia has been associated with the pathogenesis of renal fibrosis, we tested the spatial distribution of hypoxia-responsive gene signatures (**Supplemental Figure S5)**. This included a curated gene ontology set composed of 179 genes (GO:0001666, response to hypoxia) and a cancer-derived hypoxia signature with 51 genes.[22] Both gene signatures were positively enriched in the fibrotic regions, suggesting a role in the underlying pathogenesis.

Analysis of chemokine-based interactions driving cellular crosstalk during kidney rejection

Given the critical role of chemokines in orchestrating cellular migration and homing, we used a manually curated database (CellTalkDB) to examine human receptor-ligand (R-L) interaction pairs within specific renal compartments.[23] Specifically, we investigated chemokine receptors from four families (CXC, CC, C, and CXC3) and their corresponding ligands, comprising 181 R-L interactions. Detailed relative gene expression data for these genes can be found in **Supplemental Table S3**. Overall, we observed spatial co-localization between receptors and ligands in all samples (**Figure 5 and Supplemental Table S4**). One prominent finding was the frequent co-expression of ligands associated with CXCR4, such as *MIF*, *HMGB1*, and *CXCL12*. In contrast, we identified several R-L interaction pairs, specifically those involving some ligands of the CC receptor family (CCR1, CCR2, CCR5, and CCR7), that were selectively prevalent in rejection cases, particularly in the biopsy exhibiting heightened interstitial inflammation.

We also investigated the potential association of R-L expression patterns with the previously observed specific cell compartmentalization of plasma cells. To this end, we calculated GSEA enrichment scores of immune signatures in the barcodes where each R-L pair was co-expressed (**Supplemental Figure S6**). While our findings illustrate the similarities across samples, such as the pronounced association of MIF-CXCR4 and HMGB1-CXCR4 with B and T cells, and a distinct association of the CCL5-CXCR3 pair with plasma cells, they also revealed certain discrepancies that highlight the underlying cellular heterogeneity of rejection and the difficulty of drawing definitive conclusions from these results.

Exploring the biological significance of transcriptional signatures associated with kidney allograft rejection

While previous studies have identified various transcriptional signatures through microarray analysis of whole biopsies, we face the challenge of understanding the biological implications of, or alterations in, cellular dynamics that these changes represent within kidney rejection scenarios. This prompted us to investigate the biological significance of these transcriptional signatures using our ST analysis approach. In this study, we incorporated a series of well-established gene expression signatures associated with renal allograft rejection.

Carrying out GSEA enabled us to calculate enrichment scores for each unsupervised cluster obtained through our segmentation analysis of the samples (**Table 2**). First, we observed a general positive enrichment trend correlated with interstitial clusters found in non-rejection

and rejection biopsies. However, higher, more statistically significant enrichment scores were recorded in the latter scenario, suggesting a stronger association between these transcriptional signatures and areas denoting interstitial infiltration during active rejection processes. Conversely, in most instances, the signatures were negatively correlated with tubular structures within the kidney biopsy.

DISCUSSION

We present a proof-of-concept study with a limited number of samples that aims to explore the potential of ST for analyzing human kidney rejection. Our analysis revealed marked cellular heterogeneity within the renal interstitium, allowing us to examine the differential distribution of immune cells within biopsies. Our study also enabled us to compare the rejection transcriptomic signatures derived from bulk and ST data, providing additional biological insights. However, without further validation, our interpretations should be considered provisional and specific to the context of this study.

ST is a promising technology that may be useful in transplant research and, eventually, in clinical settings. Nonetheless, in our experience, using this technology presents some limitations that should be considered. One obvious shortcoming is the fluctuation in cell densities associated with each barcode due to the fixed 55-µm diameter of the spots of the transcriptomic map. This could have led to analytical inconsistencies between samples, especially for the more nuanced analyses (e.g., that of receptor-ligand distribution). Given the cellular complexity and density of the kidney, it will be necessary to increase the resolution while continuing to carry out the examination at the whole transcriptome-wide scale in order for ST's full potential in the kidney to be realized. Fortunately, this is a technical element in which advances are rapidly being made, and we expect this to be possible in the very near future.[24] Another essential element of our study is the use of OCT-embedded fresh-frozen biopsies. This material has the advantage that RNA integrity is well preserved, although at the cost of much poorer preservation of the tissue morphology. This is an important issue, given the intrinsic fragility of kidney tissue. While ST technologies suited for paraffin-embedded tissue do exist, the compromise between morphology preservation and obtaining high-quality RNA needs careful consideration when designing experiments.

ST and single-cell RNA sequencing are usually integrated to extract more comprehensive biological information. However, the variability in clinical presentations from patient to patient underlines the advantage of deriving both datasets from the same biopsy, despite the technical challenges this poses with clinical samples. This makes the selection of sequencing data sources for integration a crucial matter, as it may significantly influence the observed spatial distribution of pertinent cell types. Finally, it is important to mention that the inherent complexity and expense associated with ST are significant considerations, especially in the clinical environment. As the technology advances, it will become clearer how feasible and effective spatial transcriptomics can be in this context.

AUTHOR CONTRIBUTIONS

RMR, CLL and BSA conceived the research and supervised all aspects of the work. CMM, IT and OB prepared the kidney biopsies. CMM and RMR performed the ST procedure. MG prepared the sequencing libraries. RMR, AMA and JEM analyzed the ST data. RMR, CMM, BSA, GBC and FM wrote the paper and contributed to data analysis. All the authors read, edited, and approved the manuscript.

ACKNOWLEDGMENTS

This study has been funded by Instituto de Salud Carlos III (ISCIII) through the projects No PI19/00184, PI20/00639 and PI22/00738 co-funded by the European Union; and RICORS2040 (RD21/0005/0017) funded by European Union with charge to Next Generation EU funds, which support the actions of the Mecanismo de Recuperación y Resiliencia (MRR). The study has also been supported by PCTI-Plan de Ciencia, Tecnología e Innovación 2021-2023 from Gobierno del Principado de Asturias ("Ayudas para Grupos de Investigación del Principado de Asturias 2021-2023", FICYT, Grant number IDI/2021/000032), co-funded by FEDER Funding Program from the European Union; and by Miguel Servet I´ program (grant number CP18/00106 to B.S.-A.) from ISCIII co-funded by the European Union (EFS). RMR was supported by the Scientific Foundation of the Spanish Association Against Cancer (INVES222995RODR).

DISCLOSURE

The authors of this manuscript have no conflicts of interest to disclose as described by the American Journal of Transplantation.

DATA AVAILABILITY STATEMENT

All raw data were submitted to the NCBI Gene Expression Omnibus under accession number GSE245870.

FIGURE LEGENDS

Table 1. **Enrichment scores for immune cell subpopulations in human kidney allograft biopsies.**

Table 2. **Enrichment scores for transcriptional gene expression signatures associated with kidney allograft rejection**.

Figure 1. **Spatial organization of gene expression in human kidney allograft biopsies.** (**A**) Histological staining with hematoxylin and eosin, coupled with transcriptomic analysis, reveals distinct gene expression patterns in non-rejection and acute rejection kidney allograft biopsies. Unsupervised segmentation analysis (K-means) assigns colors to different regions. (**B**) UMAP visualization of ST analysis enables cluster annotation based on known gene expression markers, providing a comprehensive view of the cellular organization within the biopsy samples. TAL, thick ascending limb; PCT, proximal convoluted tubule; CD, collecting duct; DCT, distal convoluted tubule; CNT, connecting tubule.

Figure 2. **Distribution and expression of immune cell markers in human kidney allograft biopsies.** (**A**) UMAP visualization depicting the spatial distribution of immunoglobulin expression in kidney biopsies. Expression levels are represented on a log-normalized scale. (**B**) Spatial heatmap illustrating the expression patterns of selected immune cell markers across biopsy samples.

Figure 3. **Spatial correlation analysis of immune cells and tubule cells in human kidney allograft biopsies.** (**A**) Correlation matrix revealing relationships between spatial gene expression patterns of cell-specific signatures. Cell signatures were derived from single-cell RNA sequencing of an allograft biopsy. (**B**) Spatial overlap of immune cell signatures (LB, LT, Plasma 1 and Plasma 2 cells) in rejection. PT, proximal convoluted tubule; CD, collecting duct; LOH Asc, loop of Henle ascending limb; LOH Desc, loop of Henle descending limb; Mono, monocyte.

Figure 4. **Spatial transcriptomic patterns associated with interstitial fibrosis and tubular atrophy (IFTA) in renal transplant**. (**A**) Unsupervised segmentation analysis (K-means) of spatial gene expression data and UMAP visualization. (**B**) Cluster annotation based on known gene expression markers. (**C**) Spatial overlap of immune cell signatures (B and T cells) and fibroblasts. Histopathological annotation of fibrotic regions is indicated by boxes. (**D**) Correlation matrix of cell-specific gene expression signatures. (**E**) Spatial gene expression of a gene set from the Mouse Ageing Cell Atlas, consisting of the top 20 upregulated and top 20 downregulated genes in aged kidney tissue, and a human kidney aging signature comprising 19 upregulated and 18 downregulated genes. UMAP visualization shows average log-normalized expression of upregulated and downregulated senescence-associated genes. GSEA shows normalized enrichment scores in the fibrotic and non-fibrotic clusters. Specific expression of each gene is represented in the heatmap as $\log_2$-fold change. PT, proximal convoluted tubule; CD, collecting duct; LOH Asc, loop of Henle ascending limb; LOH Desc, loop of Henle descending limb; Mono, monocyte.

Figure 5. **Chemokine-based interactions driving cellular crosstalk during kidney rejection**. Heatmap showing spatial co-expression of chemokine receptors and ligands. Within each cluster, co-expression levels are quantified by calculating the percentage of spots in which receptor and ligand signals are both detected. Only the top 25 interactions in each sample are included in the heatmap. TAL, thick ascending limb; PCT, proximal convoluted tubule; CD, collecting duct; DCT, distal convoluted tubule; CNT, connecting tubule.

SUPPLEMENTARY MATERIAL

Supplemental Table S1. **Banff criteria scores for examined kidney allograft biopsy samples**.

Supplemental Table S2. **Marker genes for immune cell subpopulations in human kidney allograft biopsies**.

Supplemental Table S3. Chemokine receptor-ligand gene expression in kidney rejection. The table shows the relative expression of all receptors and ligands in each cluster.

Supplemental Table S4. Chemokine receptor-ligand interactions in kidney rejection. The table shows the percentage of spots in each cluster in which receptor and ligand signals both are detected, highlighting key interactions involved in immune cell recruitment and localization processes.

Supplemental Figure S1. Correlation of spatial transcriptomic clusters with histological features in kidney allograft biopsies. This figure juxtaposes ST maps with histological features of kidney allograft biopsies within specific tissue biopsies. It highlights the correspondence between transcriptomic data and underlying tissue morphology, including that of glomeruli, arteries, and fibrotic and tubulitis areas.

Supplemental Figure S2. **Comparison of unsupervised segmentation analysis with previously published spatial transcriptomic data.** Comparison of unsupervised segmentation analysis with previously published ST data. The figure compares our unsupervised segmentation results of the rejection A sample with a previous ST study. Expression signatures associated with six clusters from the previous study were used for the comparison. Signature expression in each cluster is shown as the $\log_2$-normalized average expression. Our results showed strong correlation patterns, particularly in non-rejection and acute rejection samples for interstitium and glomeruli clusters. Acute rejection samples were more closely correlated with tubular clusters than were non-rejection cases. The blood vessel cluster in the non-rejection sample displayed high expression levels of previously reported signatures for glomeruli and interstitial regions, possibly due to the presence of endothelium and to perivascular fibroblast representation, respectively.

Supplemental Figure S3. **Moran's I spatial autocorrelation analysis of gene expression in renal transplant biopsies.** Moran's I is an estimate of the correlation of gene expression among neighboring spots within the tissue sections. The figure highlights that immunoglobulin-expressing cells tend to cluster together and exert their functional effects in localized areas, indicating the spatial organization of immune cell activity. Only the top 30 genes with the highest values are included in this figure.

Supplemental Figure S4. **Comparison of spatial distribution patterns derived from various single-cell expression datasets**. This figure illustrates the spatial distribution patterns of transcriptional signatures obtained from two distinct datasets. Despite the overall concordance between these datasets, disparities highlight the influence of data-source variability on spatial interpretations. These are especially evident in the distribution of proximal tubule (PT) cells within non-rejection biopsy specimen.

Supplemental Figure S5. Spatial gene expression of hypoxia-responsive gene signatures in the kidney. UMAP visualization displays the average log-normalized expression levels of genes from two hypoxia-responsive signatures: a general gene ontology set related to the response to hypoxia containing 179 genes (GO:0001666) and a specialized cancer-derived hypoxia signature comprising 51 genes. Gene Set Enrichment Analysis (GSEA) reveals normalized enrichment

scores, demonstrating differential enrichment of both hypoxia signatures in fibrotic versus non-fibrotic clusters.

Supplemental Figure S6. GSEA enrichment scores of immune signatures based on R-L co-expression patterns. Results of Gene Set Enrichment Analysis (GSEA) for immune signatures within the barcodes where each receptor-ligand (R-L) pair was co-expressed, for the purpose of understanding the relationship between R-L expression patterns and the specific compartmentalization of immune cells. Enrichment scores are portrayed for different immune cell signatures across the rejection biopsies, including B, T, mastocytes, monocytes, and plasma cells.

REFERENCE

1. Mudiayi D, Shojai S, Okpechi I, et al. Global Estimates of Capacity for Kidney Transplantation in World Countries and Regions. *Transplantation*. 2022;106(6). doi:10.1097/TP.0000000000003943

2. Helanterä I, Räihä J, Finne P, Lempinen M. Early failure of kidney transplants in the current era—a national cohort study. *Transplant International*. 2018;31(8). doi:10.1111/tri.13115

3. Larsson L, Frisén J, Lundeberg J. Spatially resolved transcriptomics adds a new dimension to genomics. *Nat Methods*. 2021;18(1). doi:10.1038/s41592-020-01038-7

4. Torres IB, Reisaeter A V, Moreso F, et al. Tacrolimus and mycophenolate regimen and subclinical tubulo-interstitial inflammation in low immunological risk renal transplants. *Transpl Int*. 2017;30(11):1119-1131. doi:10.1111/tri.13002

5. Loupy A, Haas M, Roufosse C, et al. The Banff 2019 Kidney Meeting Report (I): Updates on and clarification of criteria for T cell– and antibody-mediated rejection. *American Journal of Transplantation*. 2020;20(9):2318-2331. doi:10.1111/ajt.15898

6. Zheng GXY, Terry JM, Belgrader P, et al. Massively parallel digital transcriptional profiling of single cells. *Nat Commun*. 2017;8. doi:10.1038/ncomms14049

7. Wu H, Malone AF, Donnelly EL, et al. Single-cell transcriptomics of a human kidney allograft biopsy specimen defines a diverse inflammatory response. *Journal of the American Society of Nephrology*. 2018;29(8):2069-2080. doi:10.1681/ASN.2018020125

8. Subramanian A, Tamayo P, Mootha VK, et al. Gene set enrichment analysis: A knowledge-based approach for interpreting genome-wide expression profiles. *Proc Natl Acad Sci U S A*. 2005;102(43). doi:10.1073/pnas.0506580102

9. Halloran PF, Venner JM, Famulski KS. Comprehensive Analysis of Transcript Changes Associated With Allograft Rejection: Combining Universal and Selective Features. *American Journal of Transplantation*. 2017;17(7):1754-1769. doi:10.1111/ajt.14200

10. Chamoun B, Caraben A, Torres IB, et al. A rejection gene expression score in indication and surveillance biopsies is associated with graft outcome. *Int J Mol Sci*. 2020;21(21). doi:10.3390/ijms21218237

11. O'Connell PJ, Zhang W, Menon MC, et al. Biopsy transcriptome expression profiling to identify kidney transplants at risk of chronic injury: a multicentre, prospective study. *The Lancet*. 2016;388(10048). doi:10.1016/S0140-6736(16)30826-1

12. Shaw BI, Cheng DK, Acharya CR, et al. An age-independent gene signature for monitoring acute rejection in kidney transplantation. *Theranostics*. 2020;10(15). doi:10.7150/thno.42110

13. Shah Y, Yang H, Mueller FB, et al. Transcriptomic signatures of chronic active antibody-mediated rejection deciphered by RNA sequencing of human kidney allografts. *Kidney Int*. 2024;105(2):347-363. doi:10.1016/j.kint.2023.11.012

14. Khatri P, Roedder S, Kimura N, et al. A common rejection module (CRM) for acute rejection across multiple organs identifies novel therapeutics for organ transplantation. *Journal of Experimental Medicine*. 2013;210(11):2205-2221. doi:10.1084/jem.20122709

15. Modena BD, Kurian SM, Gaber LW, et al. Gene Expression in Biopsies of Acute Rejection and Interstitial Fibrosis/Tubular Atrophy Reveals Highly Shared Mechanisms That Correlate With Worse Long-Term Outcomes. *American Journal of Transplantation*. 2016;16(7):1982-1998. doi:10.1111/ajt.13728

16. Ilicic T, Kim JK, Kolodziejczyk AA, et al. Classification of low quality cells from single-cell RNA-seq data. *Genome Biol*. 2016;17(1). doi:10.1186/s13059-016-0888-1

17. Ferreira RM, Sabo AR, Winfree S, et al. Integration of spatial and single-cell transcriptomics localizes epithelial cell- immune cross-talk in kidney injury. *JCI Insight*. 2021;6(12). doi:10.1172/jci.insight.147703

18. Xia C, Fan J, Emanuel G, Hao J, Zhuang X. Spatial transcriptome profiling by MERFISH reveals subcellular RNA compartmentalization and cell cycle-dependent gene expression. *Proc Natl Acad Sci U S A*. 2019;116(39). doi:10.1073/pnas.1912459116

19. Hansen J, Sealfon R, Menon R, et al. A reference tissue atlas for the human kidney. *Sci Adv*. 2022;8(23). doi:10.1126/sciadv.abn4965

20. Almanzar N, Antony J, Baghel AS, et al. A single-cell transcriptomic atlas characterizes ageing tissues in the mouse. *Nature*. 2020;583(7817):590-595. doi:10.1038/s41586-020-2496-1

21. Rowland J, Akbarov A, Eales J, et al. Uncovering genetic mechanisms of kidney aging through transcriptomics, genomics, and epigenomics. *Kidney Int*. 2019;95(3):624-635. doi:10.1016/j.kint.2018.10.029

22. Buffa FM, Harris AL, West CM, Miller CJ. Large meta-analysis of multiple cancers reveals a common, compact and highly prognostic hypoxia metagene. *Br J Cancer*. 2010;102(2):428-435. doi:10.1038/sj.bjc.6605450

23. Shao X, Liao J, Li C, Lu X, Cheng J, Fan X. CellTalkDB: A manually curated database of ligand-receptor interactions in humans and mice. *Brief Bioinform*. 2021;22(4). doi:10.1093/bib/bbaa269

24. Bressan D, Battistoni G, Hannon GJ. The dawn of spatial omics. *Science (1979)*. 2023;381(6657). doi:10.1126/science.abq4964

Table 1. Immune cell enrichment in allograft kidney biopsies.

	B cells	T cells	Mon. 1	Mon. 2	Mast.	Plas. 1	Plas. 2
Non-rejection							
Mixed (TAL)	-1.56*	-1.43	-1.24	-1.42*	-1.38*	-1.41	-1.40
Mixed (PT)	-1.77**	-1.76**	-1.28	-1.49*	-1.51*	-1.53*	-1.40
Interstitium	**2.11****	**2.19****	**1.86****	**1.93****	**1.35***	**1.57***	1.33
Blood Vessels	**1.60***	**1.69***	-0.79	1.45	1.15	1.10	-1.08
Glomeruli	-1.29	-1.45	1.05	-1.10	1.18	0.84	1.25
Acute rejection A							
Tb. and cell death	-1.39*	-1.74**	-1.43*	0.75	-1.43*	1.61	1.11
Interstitium	**2.29****	**2.33****	**2.12****	**2.23****	**1.72***	**2.09****	**2.09****
TAL	-2.16**	-2.14**	-1.35	-1.58	-1.63	-1.98*	-2.04*
Mixed (DCT/CNT/CD)	-1.72*	-1.61*	-2.18**	-1.95**	-1.19	-1.88**	-1.93**
PCT	1.10	1.16	1.26	1.17	-1.20	-2.12**	-2.11**
Glomeruli	-1.74*	-1.61	-1.25	-1.54	**1.41***	-1.93*	-1.94*
Acute rejection B							
Plasma cell enriched	-1.17	-1.52**	0.82	0.79	-1.54**	**1.89***	**1.93****
Mixed (Glom./Inter.)	**2.10****	**2.21****	**1.44***	**1.9****	**1.74****	-2.10**	-2.17**
Mixed (TAL/ DCT/CNT/CD)	-1.88*	-2.31**	1.31	-1.57	1.34	-2.16**	-2.18**
PCT	-2.32**	-2.26**	-2.06*	-2.11*	-1.81*	-1.63*	1.14

Table 2. Enrichment scores for transcriptional gene expression signatures associated with kidney allograft rejection.

	O'Connell et al. 2016	Shaw et al. 2020	Halloran et al. 2017	Chamoun et al. 2020	Shah et al. 2024	Khatri et al. 2013	Modena et al. 2016
Non-rejection							
Mixed (TAL)	-0.54	-1.43	-1.26	-1.15	-1.12	-1.38	**-1.50***
Mixed (PT)	-0.51	-1.27	-0.86	-0.64	-0.98	-1.16	-1.28
Interstitium	0.87	1.00	1.15	1.34	1.34	**1.69****	1.24
Blood Vessels	0.79	1.48	-0.95	0.37	0.91	-0.83	1.40
Glomeruli	-0.45	0.64	1.19	0.56	0.69	1.06	0.81
Acute rejection (A)							
Tubulitis and cell death	-0.87	-1.33	-1.39	-0.79	-0.70	**-1.41***	-1.27
Interstitium	**1.63***	1.04	**2.11****	**2.03****	**2.04****	**1.84***	**2.02****
TAL	-0.82	-1.48	-1.67	-1.63	-1.84	-1.75	-1.25
Mixed (DCT/CNT/CD)	-1.07	**-1.64***	**-1.81****	**-1.52***	**-1.81****	**-1.86****	**-2.09****
PCT	-0.86	-0.86	0.89	-1.12	1.19	-1.16	-1.01
Glomeruli	-0.94	**1.55***	-0.78	-1.22	-1.46	**1.50***	-1.10
Acute rejection (B)							
Plasma cell enriched	0.59	-0.39	**-1.94***	1.28	0.84	-0.92	1.20
Mixed (Glomer./Interest.)	1.54	**1.69***	**1.75****	**1.51***	1.08	**1.78****	1.23
Mixed (TAL/ DCT/CNT/CD)	-1.43	-1.21	-1.49	**-1.88***	1.39	-1.18	**-1.80***
PCT	-1.32	-1.36	**-1.93***	**-2.07***	**-1.76***	**-1.94***	-1.21
i-IFTA							
Non-fibrotic	-0.84	-1.00	-1.10	-0.92	-1.68	-1.50	-1.17
Fibrotic	0.84	1.01	1.10	0.91	1.68	1.51	1.18

A

Non-rejection

H&E

SPOTS (K-means)

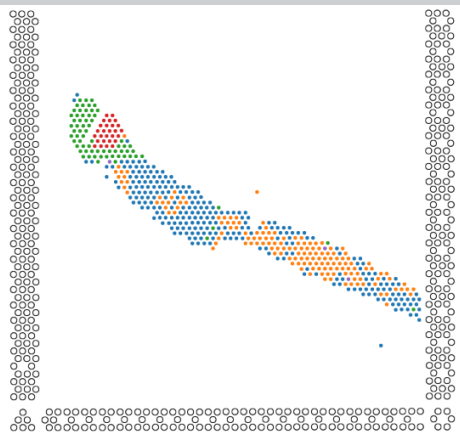

Rejection (A)

H&E

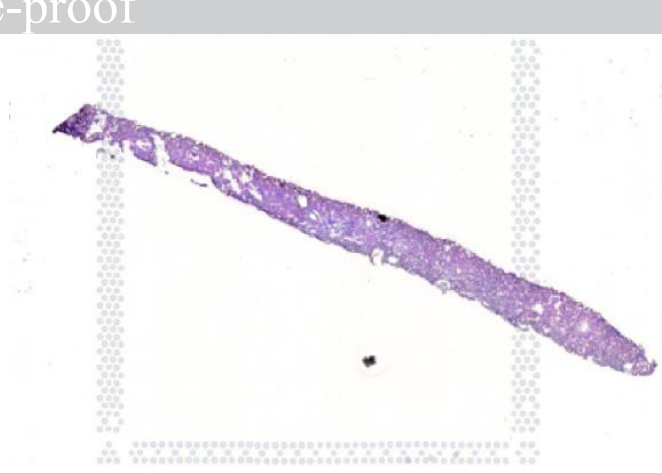

SPOTS (K-means)

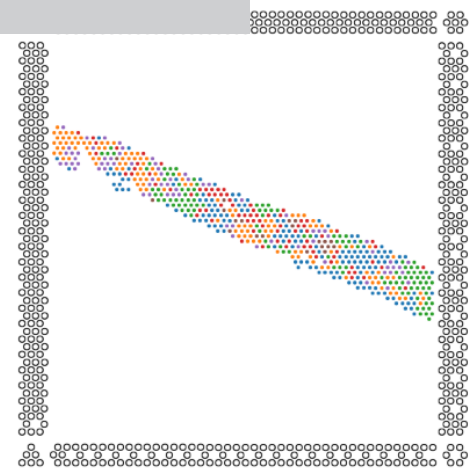

Rejection (B)

H&E

SPOTS (K-means)

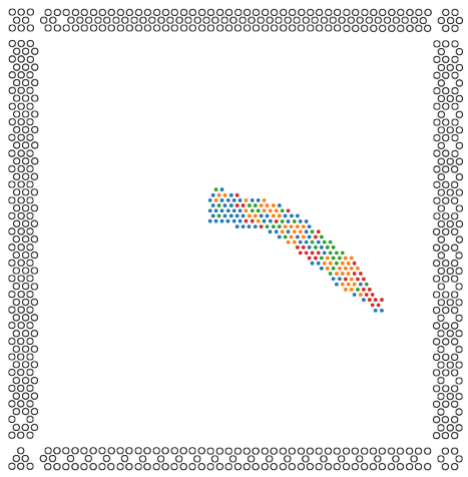

B

Non-rejection

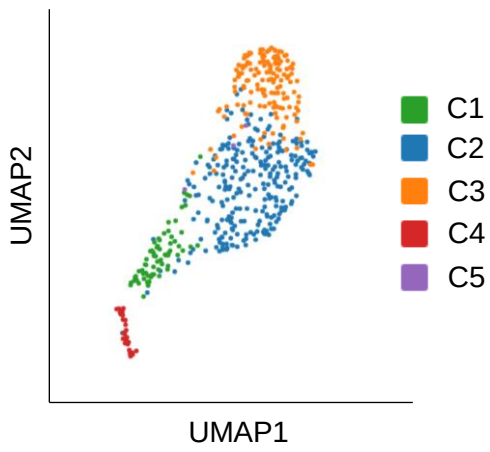

Rejection (A)

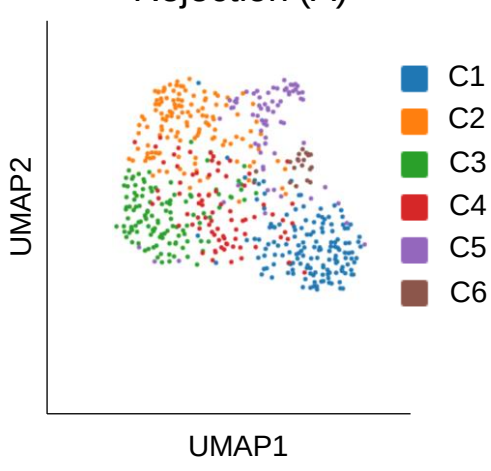

Rejection (B)

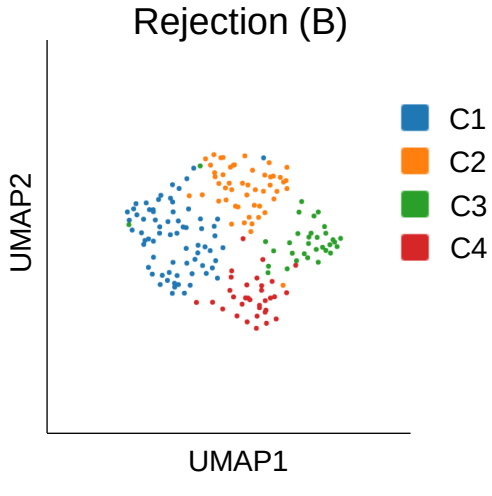

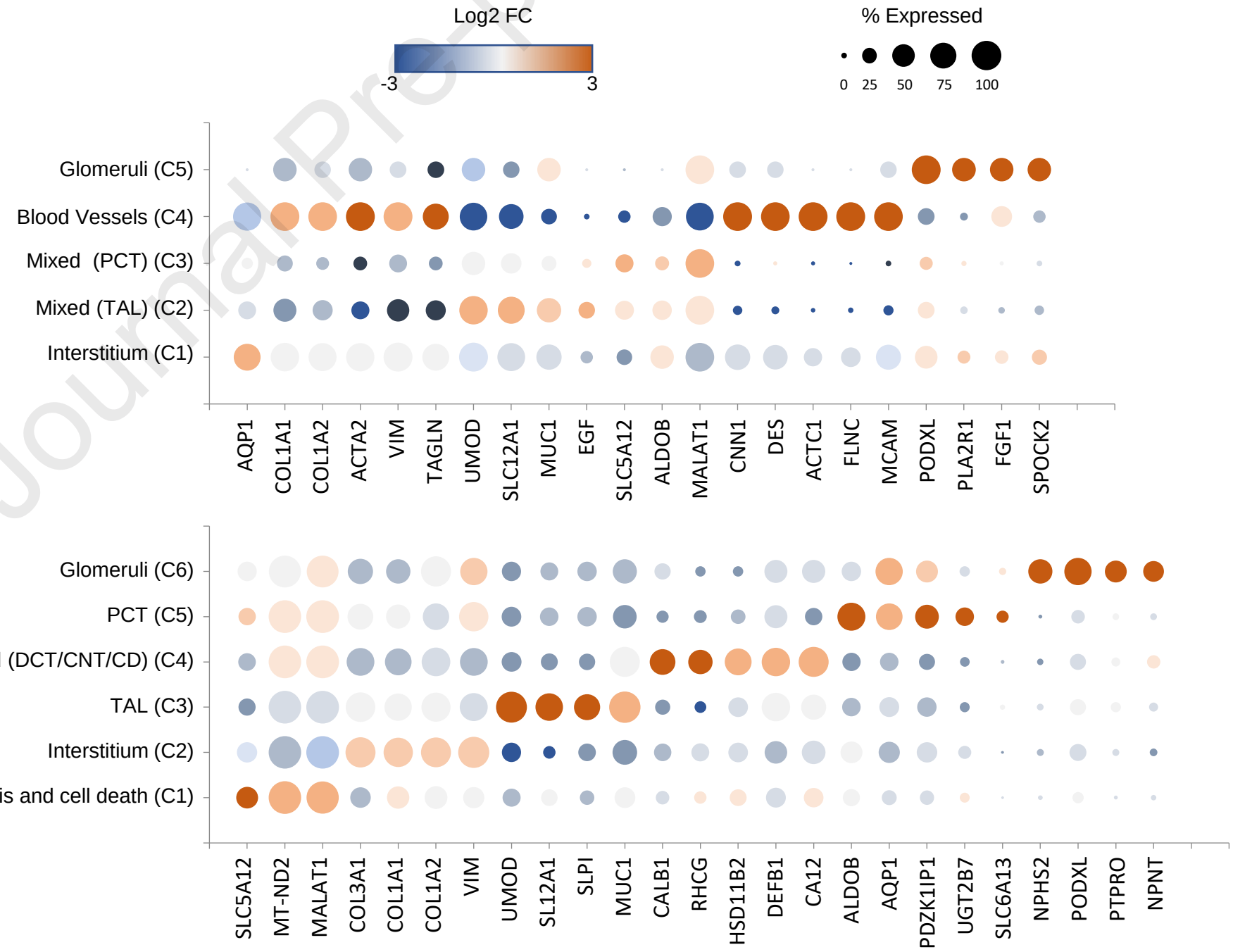

A

Non-rejection

Rejection (A)

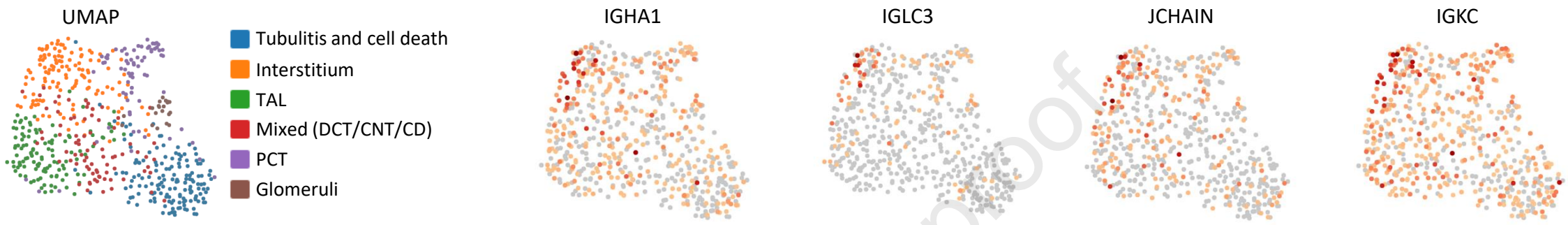

Rejection (B)

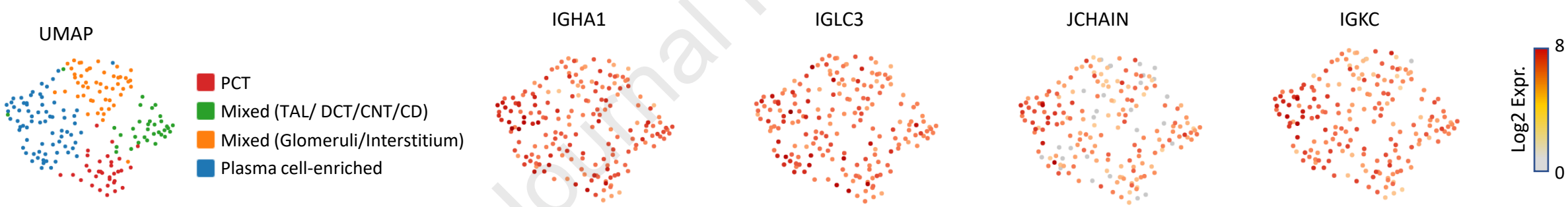

B

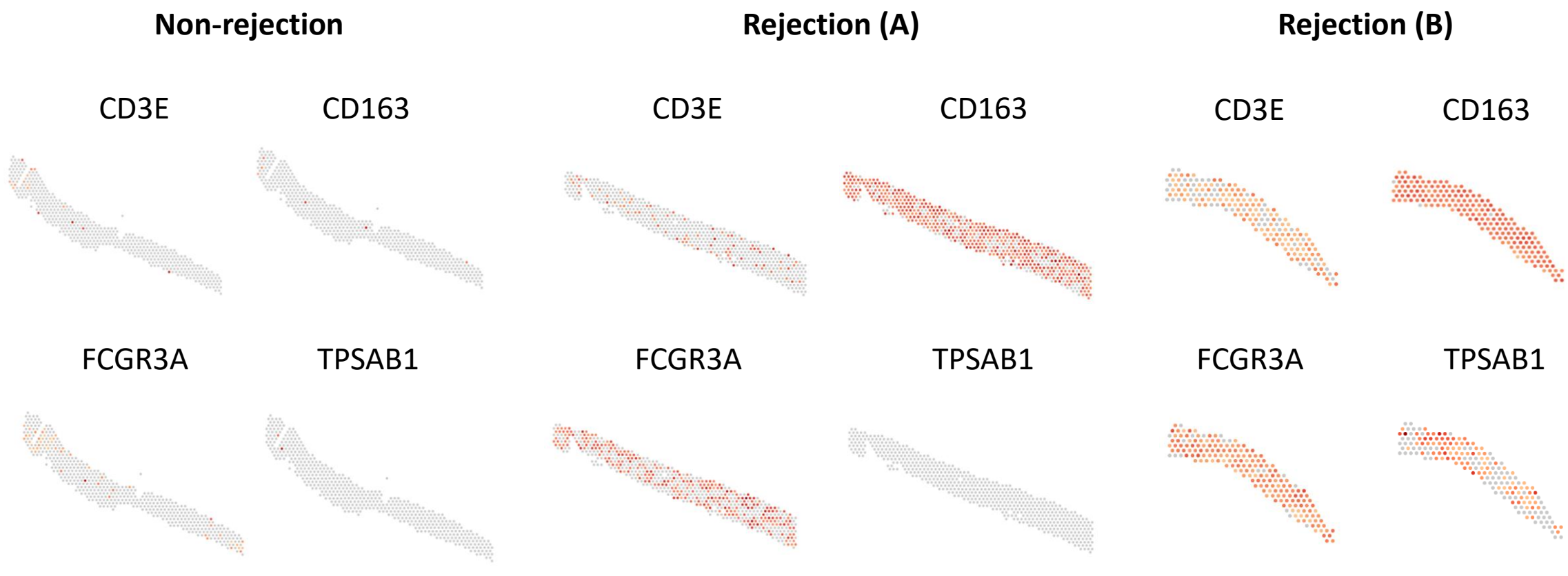

A

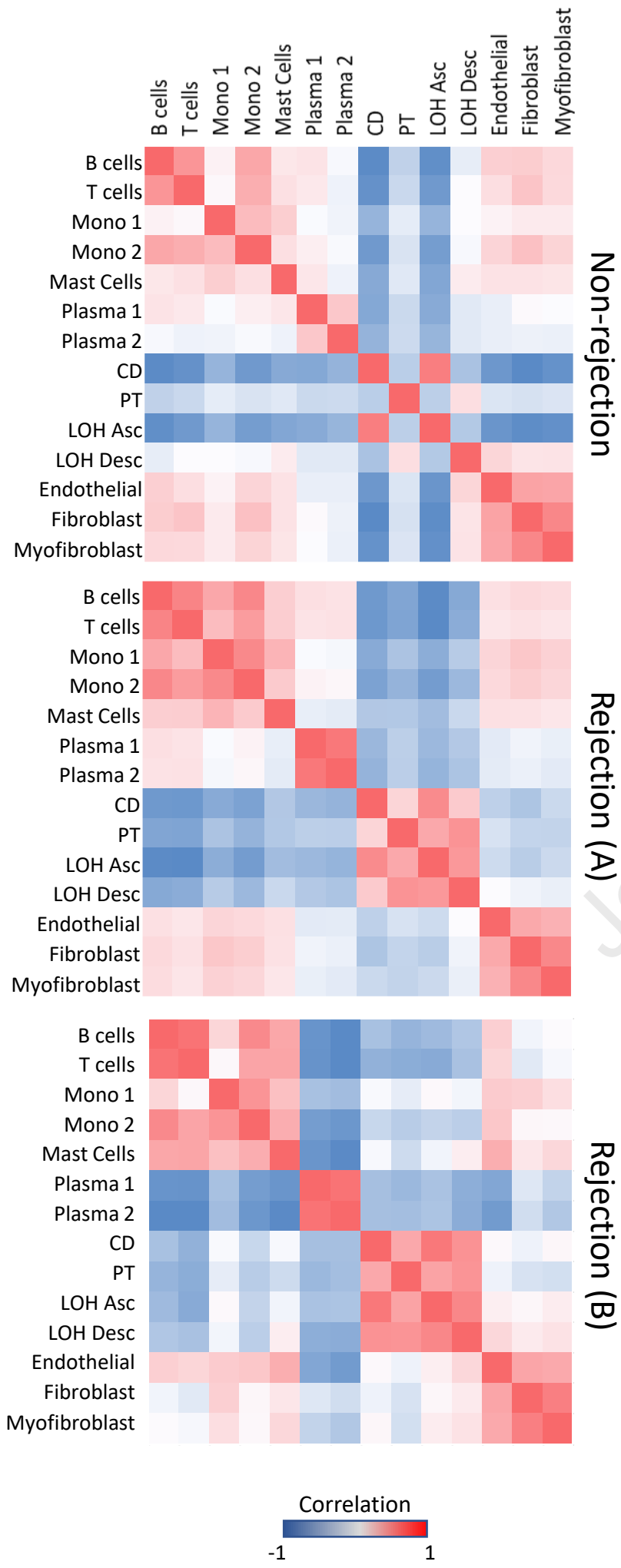

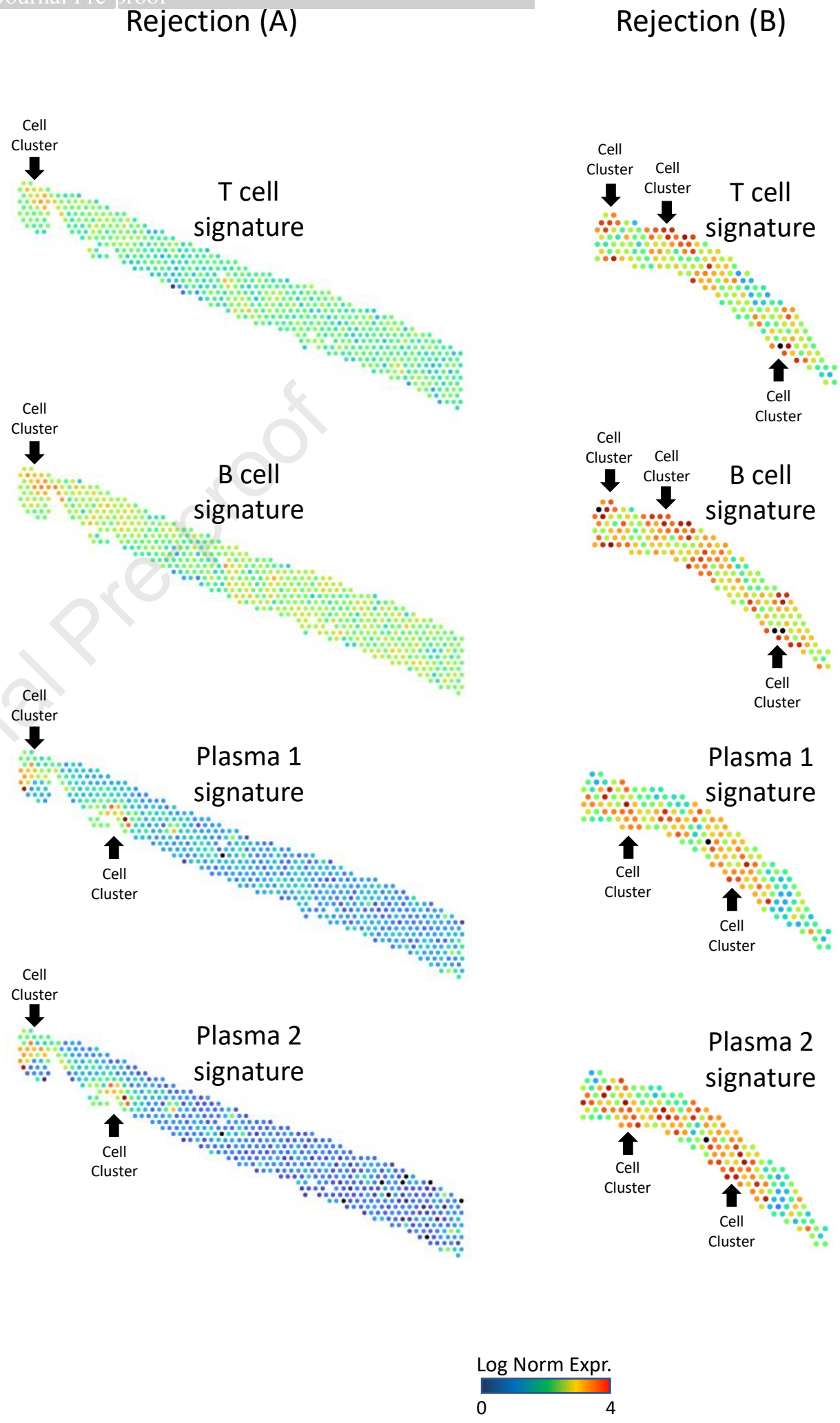

A

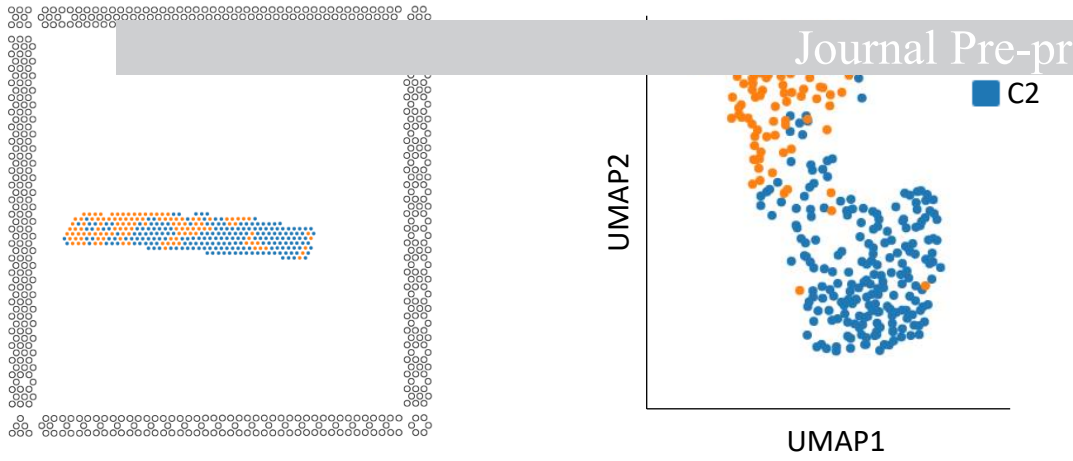

C

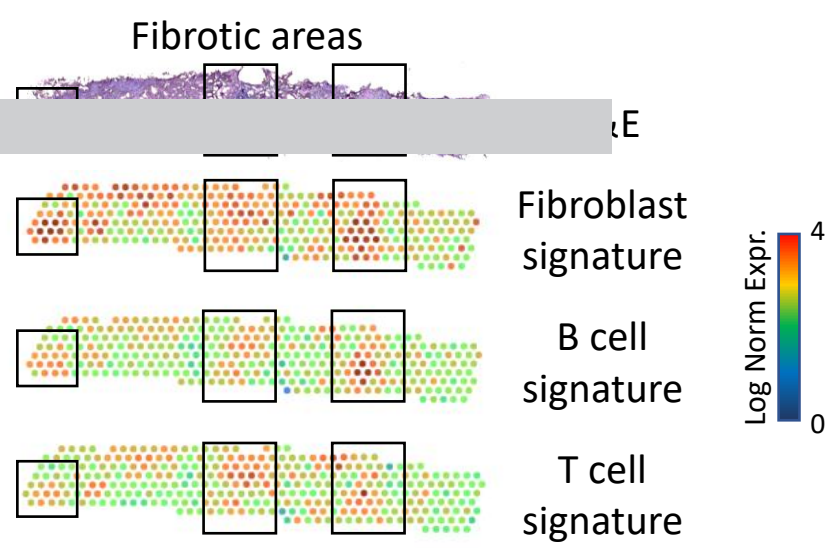

B

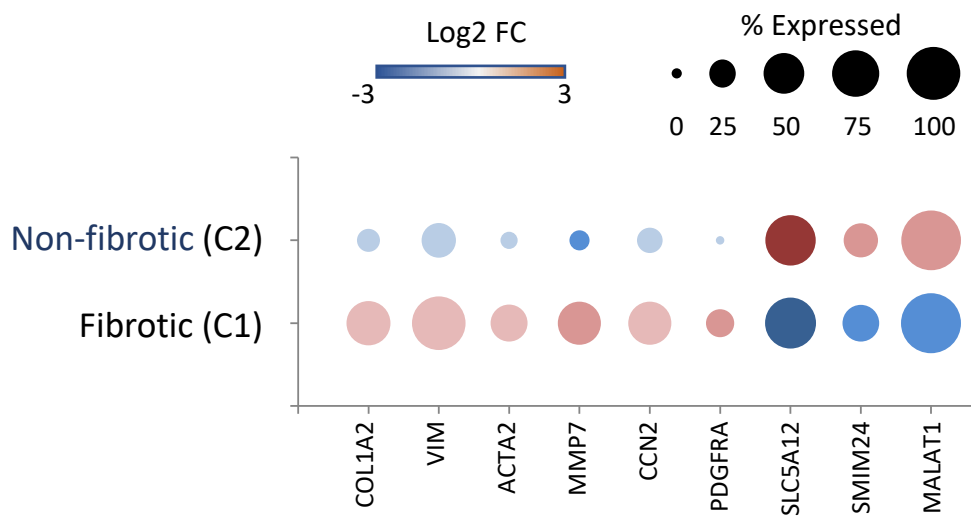

D

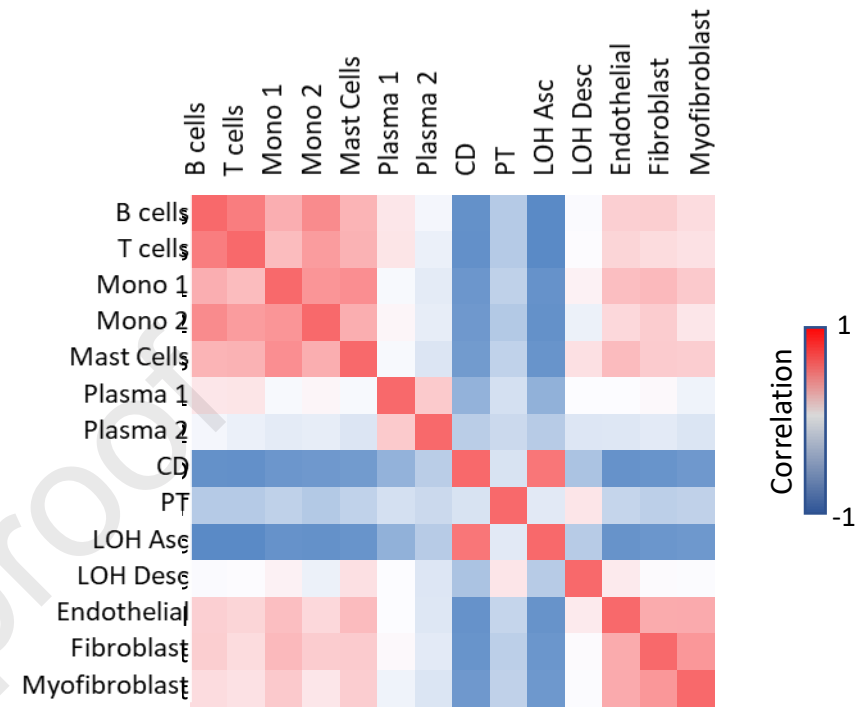

E

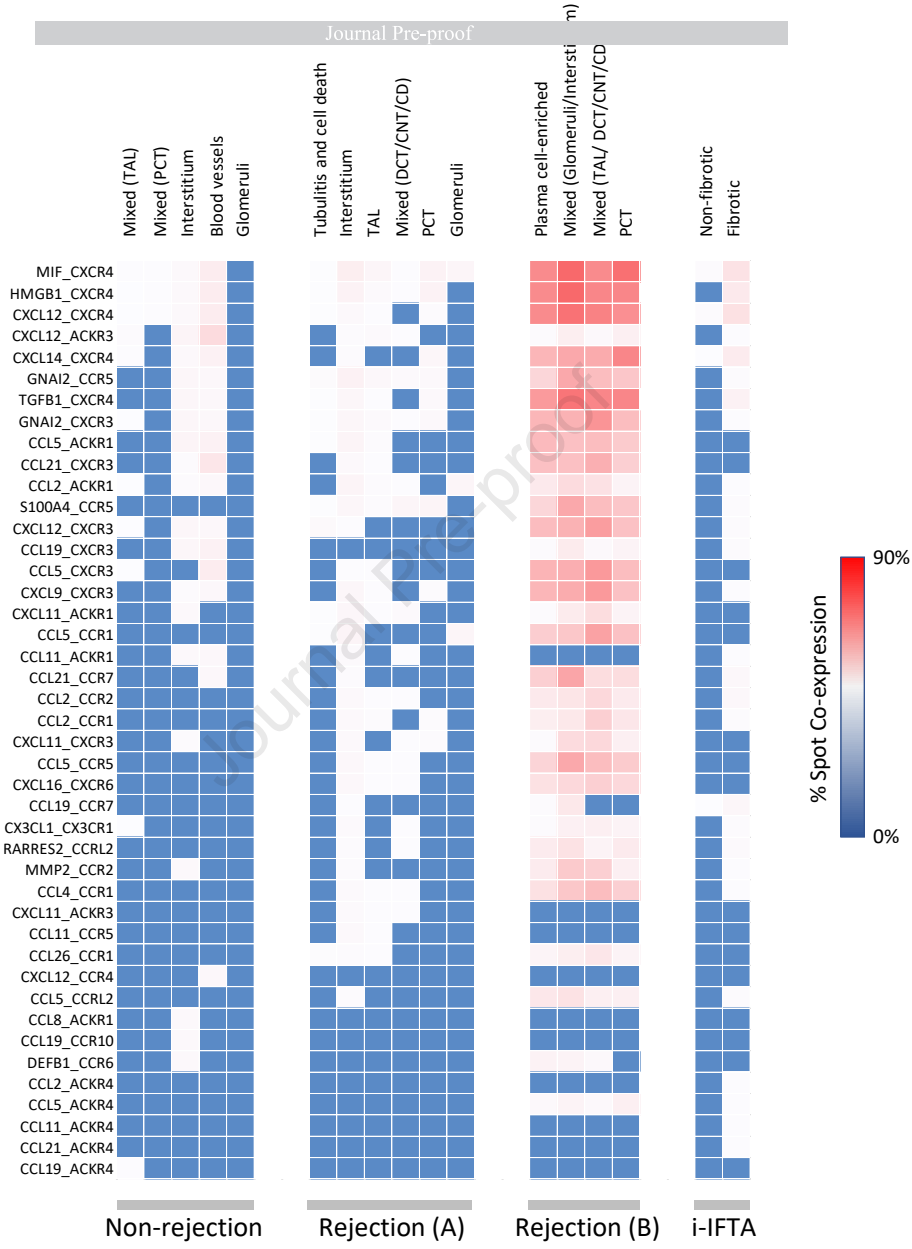

Declaration of interests

☒ The authors declare that they have no known competing financial interests or personal relationships that could have appeared to influence the work reported in this paper.

☐ The authors declare the following financial interests/personal relationships which may be considered as potential competing interests: